Nanoscale

PAPER

View Article Online
View Journal | View Issue

Cite this: *Nanoscale*, 2019, **11**, 2027

A tungsten nitride-based degradable nanoplatform for dual-modal image-guided combinatorial chemo-photothermal therapy of tumors†

Cheng Zhang,‡[a] Shi-Bo Wang,‡[a,b] Zhao-Xia Chen,[a] Jin-Xuan Fan,[a] Zhen-Lin Zhong*[a] and Xian-Zheng Zhang *[a,b]

Received 9th November 2018,
Accepted 21st December 2018

DOI: 10.1039/c8nr09064e

rsc.li/nanoscale

An innovative tungsten-based multifunctional nanoplatform composed of polyethylene glycol (PEG)-modified tungsten nitride nanoparticles (WN NPs) is constructed for tumor treatment. The PEG-WN NPs not only possess strong near-infrared (NIR) absorbance, high photothermal conversion efficiency, and excellent photothermal stability, but also effectively inhibit tumor cells upon 808 nm laser irradiation. After coating with thiolated (2-hydroxypropyl)-β-cyclodextrin (MUA-CD) on the surface, such a nanoplatform can also be used for drug delivery (such as DOX) and presents a synergistic tumor inhibition effect both *in vitro* and *in vivo*. Furthermore, the PEG-WN NPs present good contrasting capability for X-ray computed tomography (CT) and photoacoustic (PA) imaging. With PA/CT imaging, the tumor can be accurately positioned for precise treatment. It is worth mentioning that PEG-WN NPs are biodegradable and could be effectively excreted from the body with no appreciable toxicity *in vivo*. It is expected that this biocompatible multifunctional nanoplatform can serve as a potential candidate for tumor treatment in future clinical applications.

Introduction

As a non-conventional treatment of tumors, photothermal therapy (PTT) has attracted considerable attention due to its outstanding advantages, such as low cost, high selectivity and minimal invasiveness.[1–4] Upon near-infrared (NIR) light irradiation, the photothermal agents (PTAs) applied in PTT are expected to generate hyperthermia rapidly, which could efficiently induce thermal ablation of tumors. In the last few decades, plenty of materials, especially inorganic nano-agents with strong NIR absorbance, have been intensively investigated for PTT.[5–10] Different from conventional NIR dyes, inorganic nano-agents present better photostability, higher tumor enrichment degree by the enhanced permeability and retention (EPR) effect and improved pharmacokinetics.[11–13] However, many inorganic formulations are not biodegradable, and their clinical applications have often been limited by the long-term biosafety concerns.[14,15] So it is of great significance to develop inorganic nano-agents with good biodegradability for PTT. Apart from this, because of the irregular growth and abnormal functions of tumor vessels, the accumulation of PTAs in tumor tissues is always inhomogeneous, leading to ineffective dissipation of heat and resulting in incomplete tumor inhibition.[16] To solve this problem, a feasible solution is to further use PTAs as drug carriers to combine PTT with chemotherapy, which is considered to be able to improve the therapeutic efficacy *versus* a single treatment.[17–19]

Among the inorganic PTAs, metal-based substances account for a considerable proportion and tungsten (W)-based nano-agents are one of the important categories. Until now, different kinds of W-based nanostructures (such as WS_2, WO_3, $W_{18}O_{49}$, and Rb_xWO_3) were developed for PTT, drug delivery, and imaging.[20–27] Recently, tungsten nitride (WN), a black metallic photocatalyst, has been developed for water splitting.[28,29] On the basis of the high absorbance in the NIR region of WN and the good biocompatibility of W, WN holds great promise to be an excellent PTA for tumor treatment. However, since the real use of WN nanostructures for biomedical applications has not yet been fully investigated to date, the *in vivo* behavior of WN nanostructures is still unknown.

Here, we report on a novel theranostic nano-agent fabricated by coating WN nanoparticles (NPs) with thiol poly(ethylene glycol) (SH-PEG). With such PEG-WN NPs, we not only for

[a]*Key Laboratory of Biomedical Polymers of Ministry of Education and Department of Chemistry, Wuhan University, Wuhan 430072, P. R. China.*
E-mail: zlzhong@whu.edu.cn, xz-zhang@whu.edu.cn
[b]*The Institute for Advanced Studies, Wuhan University, Wuhan 430072, P. R. China*
†Electronic supplementary information (ESI) available. See DOI: 10.1039/c8nr09064e
‡These authors contributed equally to this work.

the first time evaluated the potential of PEG-WN NPs as PTAs for NIR hyperthermia generation and inhibition of tumor cells, but also transformed them into drug delivery systems and realized controlled drug release by acidic pH after coating thiolated (2-hydroxypropyl)-β-cyclodextrin (MUA-CD) on the surface. Furthermore, *in vivo* combinational tumor therapy and photoacoustic (PA)/X-ray computed tomography (CT) imaging were also evaluated in a mouse xenograft tumor model. The degradation and clearance behavior of PEG-WN NPs were also investigated to further verify their potential for biomedical applications. We expect our research to lay a foundation for further work in developing novel W-based nanoagents with high biocompatibility and efficiency for tumor theranostic applications.

Results and discussion

Synthesis and characterization of PEG-WN NPs

WN NPs were fabricated by a two-step route (Scheme 1). Briefly, bulk WN composed of aggregated nanoparticles (Fig. S1†) was firstly synthesized according to the literature report.[30] Then WN NPs were prepared by an ultrasonication process. X-ray diffraction (XRD) analysis confirms the crystal phase and purity of the as-prepared WN NPs (Fig. S2†). To improve the dispersibility and biocompatibility, SH-PEG was coated on the surface of WN NPs through the formation of the W–S bond.[20,31] The success of PEG coating on the NPs was confirmed by the FT-IR spectra (Fig. S3†) and X-ray photoelectron spectroscopy (XPS) spectra (Fig. S4†), indicated by the appearance of C–O peaks in both spectra. As indicated by transmission electron microscopy (TEM) (Fig. 1A), the dispersity of PEG-WN NPs was improved obviously. Meanwhile, the lattice spacing was found to be 0.207 nm under high-resolution TEM (HRTEM), which corresponds to the WN crystal structure. The elemental mapping images showed that the S and O elements were homogeneously distributed on the surface of WN (Fig. S5†). The hydrodynamic size of PEG-WN NPs was 143 nm as observed by dynamic light scattering (DLS) (Fig. 1B). Compared to the rapidly precipitated WN NPs, the as-prepared PEG-WN NPs exhibited great dispersity in water, phosphate-buffered saline (PBS), and serum (Fig. 1C). Moreover, the aqueous solution of PEG-WN NPs with a black color exhibited strong absorption from the ultraviolet (UV) to NIR region (Fig. 1D), which is highly desirable for PTT.

The NIR-induced hyperthermia of PEG-WN NPs was further evaluated in detail. As shown in Fig. 1E, upon 808 nm laser irradiation, the aqueous solution of PEG-WN NPs was heated up quickly in a concentration-dependent manner. The PEG-WN NPs solution even at a low concentration of 20 μg mL^{-1} shows an obvious temperature rise upon irradiation. Moreover, at a concentration of 60 μg mL^{-1}, the temperature of the solution was elevated by ~25 °C after only 8 min of irradiation (1 W cm^{-2}). The photothermal conversion efficiency of PEG-WN NPs was found to be about 33% (Fig. S6†), due to its strong localized surface plasmon resonance (LSPR) effect, which is higher than those of many previously reported photothermal agents (Table S1†). We further studied the NIR-induced hyperthermia with alternating variation of concentration and laser power; the ultimate temperature and heating rate changed accordingly, suggesting that the photothermal effect of PEG-WN NPs could be finely tuned

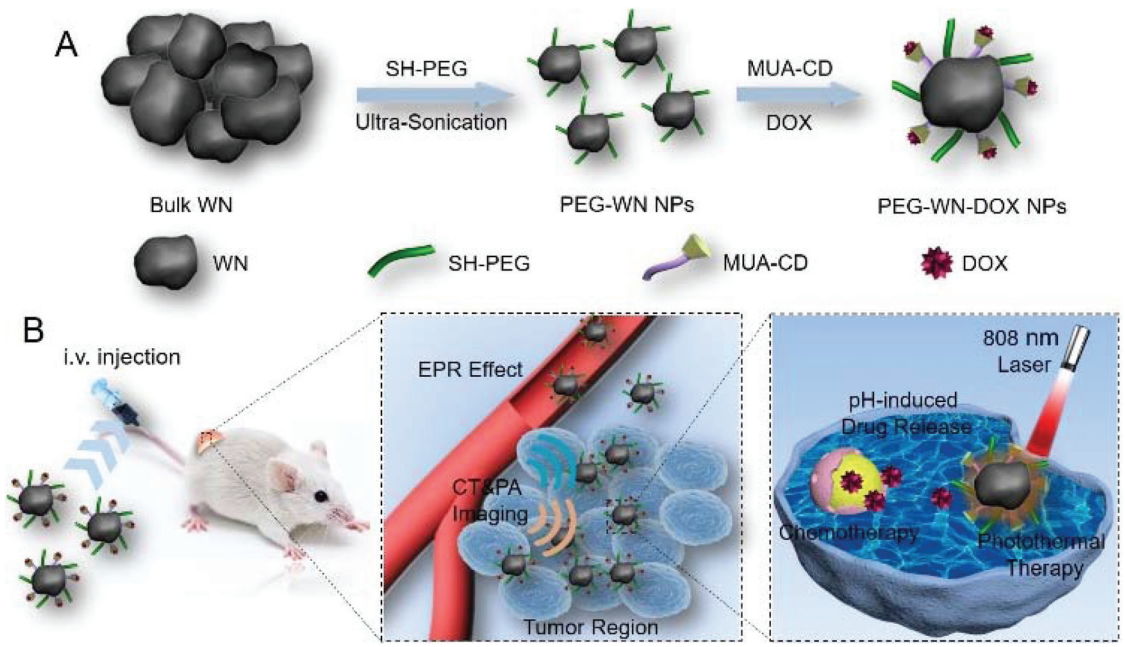

Scheme 1 Schematic illustration of (A) the fabrication process of PEG-WN NPs and (B) PEG-WN NPs for dual-modal PA/CT imaging and combinatorial chemo-photothermal therapy.

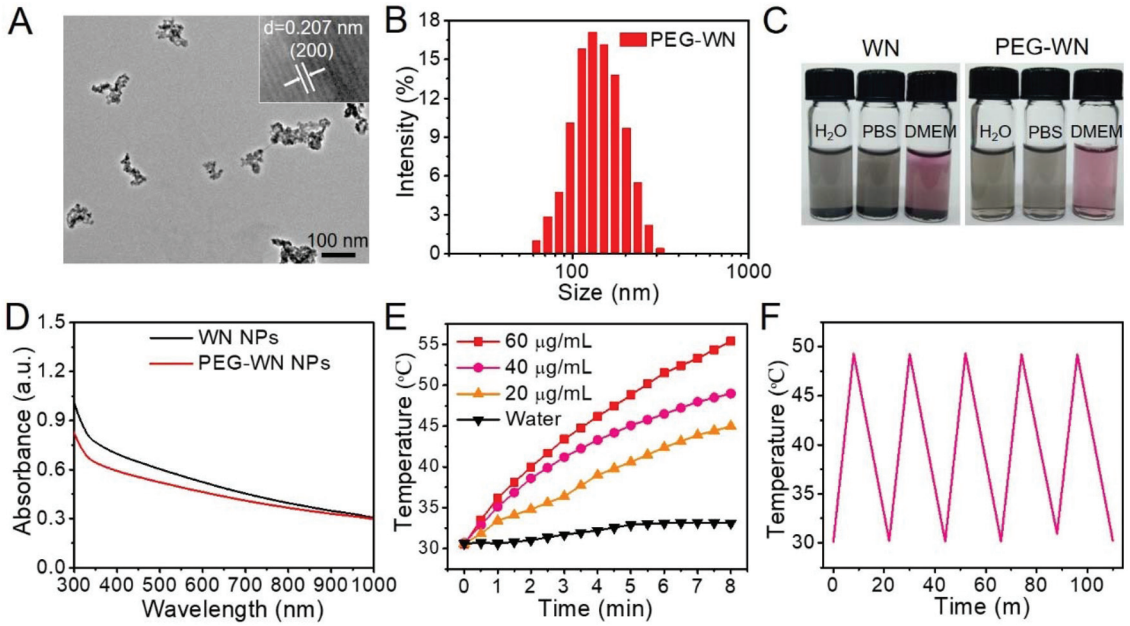

Fig. 1 (A) TEM image of PEG-WN NPs. The inset shows the corresponding HRTEM image. (B) DLS analysis of PEG-WN NPs. (C) Digital photographs of WN and PEG-WN NPs dispersion in different solutions. (D) UV/Vis-NIR absorbance spectra of WN and PEG-WN NPs in water. (E) Temperature evaluation of PEG-WN NPs with various concentrations under 808 nm laser irradiation (1 W cm^{-2}). (F) Recycling heating profile of PEG-WN NPs under 808 nm laser irradiation for 5 on/off cycles.

(Fig. S7†). Additionally, the temperature changes of the PEG-WN NPs solution presented no obvious reduction after five cycles of heating and cooling processes, demonstrating the great photothermal stability of the PEG-WN NPs (Fig. 1F). All of the results above indicate that the as-prepared PEG-WN NPs hold great potential to serve as PTAs for therapeutical applications.

Cytotoxicity and photothermal cytotoxicity

The ideal PTAs are expected to be harmless in the dark but have significant cytotoxicity after NIR light irradiation. The performance of PEG-WN NPs was then estimated in murine colorectal cancer (CT26) and breast cancer (4T1) cells *in vitro*. As shown in Fig. 2A, incubation with PEG-WN NPs for 24 h

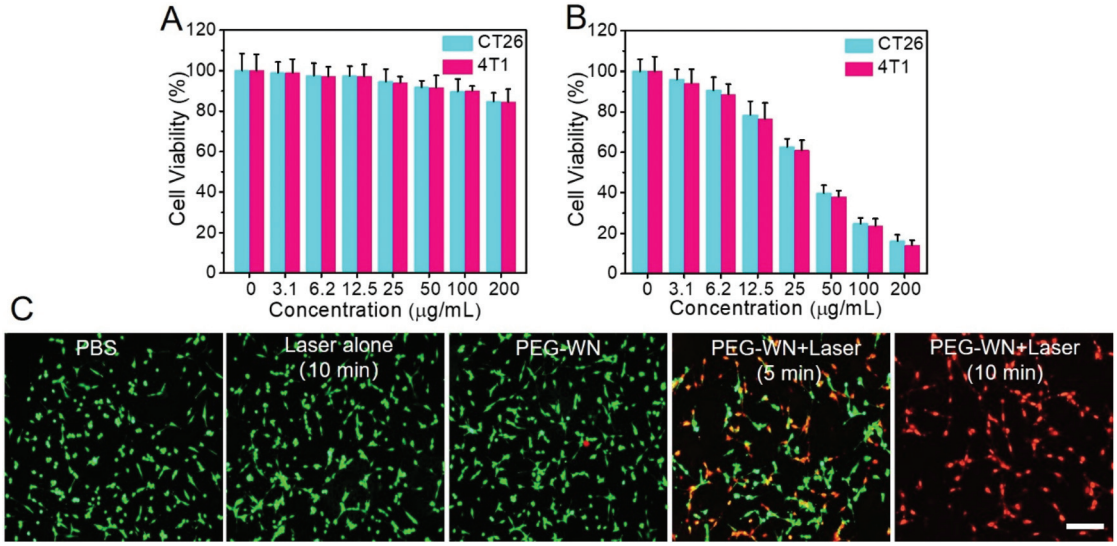

Fig. 2 (A) Cell viability of CT26 and 4T1 cells after co-incubation with PEG-WN NPs with different concentrations for 24 h. (B) Cell viability of CT26 and 4T1 cells treated with various concentrations of PEG-WN NPs and 808 nm laser irradiation (1 W cm^{-2}, 5 min). (C) Fluorescent images of calcein AM (green, live cells) and propidium iodide (red, dead cells) costained CT26 cells with different treatments (scale bar: 100 μm).

without NIR light exposure presented no significant cytotoxicity to both cell lines. The cell viabilities were still higher than 85%, and even the concentration of PEG-WN NPs reach up to 200 μg mL^{-1}; after extending the incubation time to 48 and 72 h, the cell viabilities decreased slightly (Fig. S8†). In contrast, PEG-WN NPs treated CT26 and 4T1 cells with NIR light irradiation presented an obvious dose-dependent cell death. Over 60% cells treated with the PEG-WN NPs at a concentration of 50 μg mL^{-1} were killed under irradiation after 24 h of incubation (Fig. 2B). The photothermal effect of PEG-WN NPs was further confirmed by fluorescence live/dead cell assay. As displayed in Fig. 2C, CT26 cells treated with PEG-WN NPs with NIR light irradiation were destroyed obviously, and more cells were killed upon extending the irradiation time. In contrast, almost no cell killing is observed in NIR light or PEG-WN NPs treated alone groups. Similar appearance was also observed in 4T1 cells (the data are not shown). These findings clearly indicate that the PEG-WN NPs could act as safe PTAs for different kinds of tumor cells.

In vitro drug delivery

To test the possibility of WN NPs as nanocarriers for drug delivery, the broad-spectrum and first-line anticancer drug doxorubicin (DOX) was loaded on the surface of PEG-WN NPs through thiolated MUA-CD.[32–35] The as-prepared PEG-WN-DOX NPs showed good dispersion in water with a hydrodynamic size of 156 nm measured by DLS (Fig. 3A and Table S2†). The new peaks at 1470 cm^{-1} and 1284 cm^{-1} in the infrared spectrum indicated the successful loading of DOX (Fig. S3†), which was also confirmed by UV/Vis-NIR absorbance spectra (Fig. S9†). The DOX-loading capacity was detected to be 9.8% (DOX weight ratio of the total weight of NPs). In addition, PEG-WN-DOX and PEG-WN NPs exhibited similar heating profiles in the photothermal conversion experiments, which indicated that the drug loading process had almost no influence on the photothermal effects of PEG-WN NPs (Fig. 3B). The acid-triggered release profile of DOX from PEG-WN-DOX NPs was then tested. As shown in Fig. 3C, over 70% DOX was released at pH 5.0 after 24 h. In contrast, only less than 30% DOX release was observed at pH 7.4 during the same time. Afterwards, we investigated the intracellular drug delivery ability of PEG-WN-DOX NPs to CT26 cells using confocal laser scanning microscopy. The fluorescence of DOX was observed 4 h after co-incubation with PEG-WN-DOX NPs, indicating the successful cellular internalization of the NPs (Fig. S10†). CT26 cells were treated with PEG-WN-DOX NPs at increasing concentrations with or without NIR light irradiation for the cell viability test. As shown in Fig. 3D, the cells died in a dose-dependent manner in both groups. Compared with the cells treated with PEG-WN-DOX NPs alone, many more cells were suppressed when combined with laser irradiation (1 W cm^{-2} for 5 min), resulting in nearly 85% cell death at a PEG-WN-DOX NPs concentration of 50 μg mL^{-1}. These favorable results showed that PEG-WN NPs could be easily transformed as a drug delivery system, and the as-prepared PEG-WN-DOX NPs exhibited an excellent chemo-photothermal combinational tumor inhibition effect *in vitro*.

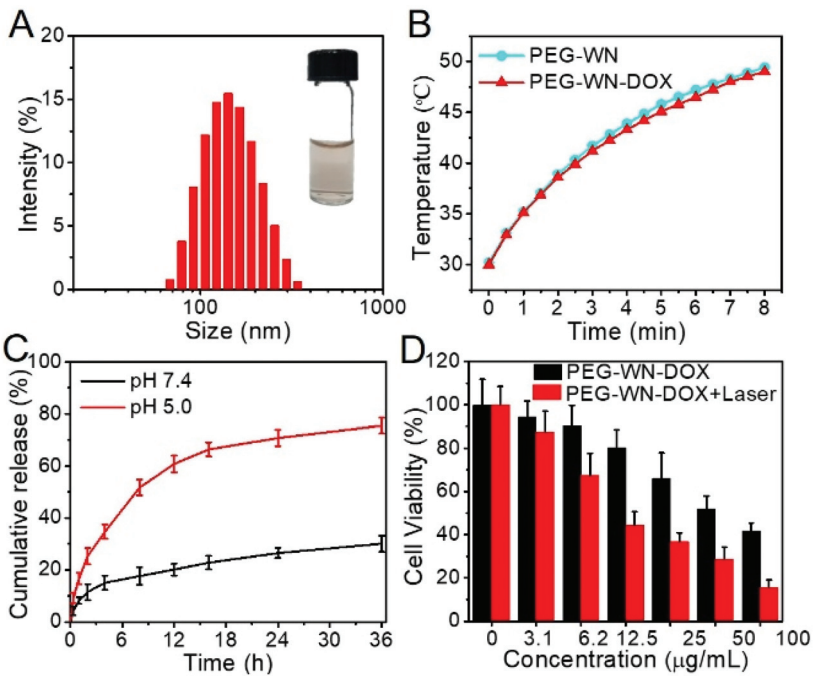

Fig. 3 (A) DLS analysis and digital photo of PEG-WN-DOX NPs in water. (B) Temperature evaluation of PEG-WN and PEG-WN-DOX NPs aqueous solution under irradiation by an 808 laser (1 W cm^{-2}). (C) The release profile of DOX from PEG-WN-DOX at different pH values. (D) Cell viability of CT26 cells treated with various concentrations of PEG-WN-DOX NPs with or without 808 nm laser irradiation (1 W cm^{-2}, 5 min).

PA and CT imaging

In addition to the efficient inhibition of tumor cells, the PEG-WN NPs with high NIR absorbance are also conjectured to exhibit excellent PA imaging performance. Since PA imaging combines the high contrast of optical imaging and deep tissue penetration of ultrasound imaging, it enables us to observe the tumor accumulation of nano-agents in deep tissues.[36] Before *in vivo* PA imaging, the PA signals from the aqueous solutions were firstly collected. As presented in Fig. 4A and B, the PA signal intensities increase linearly with the concentration of PEG-WN NPs, which is in favor of quantitative PA imaging. Next, we monitored the accumulation of PEG-WN NPs at the tumor *in vivo*. The PEG-WN NPs were intravenously injected into the CT26 tumor-bearing BALB/c mice, and then the PA signals were collected at predetermined times. The PA signals in the tumor region were very weak but increased remarkably 1 h after injection and can be detected even after 24 h (Fig. 4C and D), indicating the efficient tumor accumulation and long-term retention of PEG-WN NPs.

Apart from PA imaging, considering the high X-ray attenuation coefficient of the W element, we wonder whether PEG-WN NPs could also be utilized as efficient contrast agents for CT imaging, which is one of the most commonly used imaging tools for medical diagnosis and can provide high-resolution 3D structural details of the whole body.[31,37] To verify our speculation, their X-ray attenuation was firstly compared with that of diatrizoate sodium, a widely used CT contrast agent in the clinic. As described in Fig. 4E and F, the Hounsfield unit (HU) values also show strong linear relationship with the concentrations of the PEG-WN NPs. Notably, the slope is even larger than that of diatrizoate sodium, indicating the great contrast efficacy of PEG-WN NPs for CT imaging. Encouraged by this, we then employed PEG-WN NPs for *in vivo* CT imaging. Remarkable CT contrast signals were detected in the tumor region 24 h post PEG-WN NPs injection, which proved the enhanced permeability and retention effect of PEG-WN NPs (Fig. 4G). Both the PA and CT imaging results demonstrated the efficient accumulation of PEG-WN NPs in tumors and also suggested the potential of PEG-WN NPs for dual-modal image-guided accurate tumor treatment.

In vivo tumor inhibition

To further evaluate the *in vivo* therapeutic effect, CT26 tumor-bearing mice were randomly divided into five groups (PBS, PEG-WN NPs, PEG-WN NPs + laser, PEG-WN-DOX NPs and PEG-WN-DOX NPs + laser) for different treatments. The 808 nm laser irradiation was given 24 h post injection. The whole-body thermal images were obtained by using an infrared thermal camera. As displayed in Fig. 5A and B, the temperature of the tumor site for the PBS group increased by only less than 4 °C after NIR light irradiation, whereas the tumor temperature in the PEG-WN NPs and PEG-WN-DOX NPs groups increased by 15 °C and reached over 52 °C after the same irradiation period. These results highlighted the favorable photothermal performance of PEG-WN and PEG-WN-DOX NPs *in vivo* and also indicated their remarkable tumor selectivity. The detection result of W distribution also confirmed the selective tumor accumulation of PEG-WN NPs (Fig. S11†).

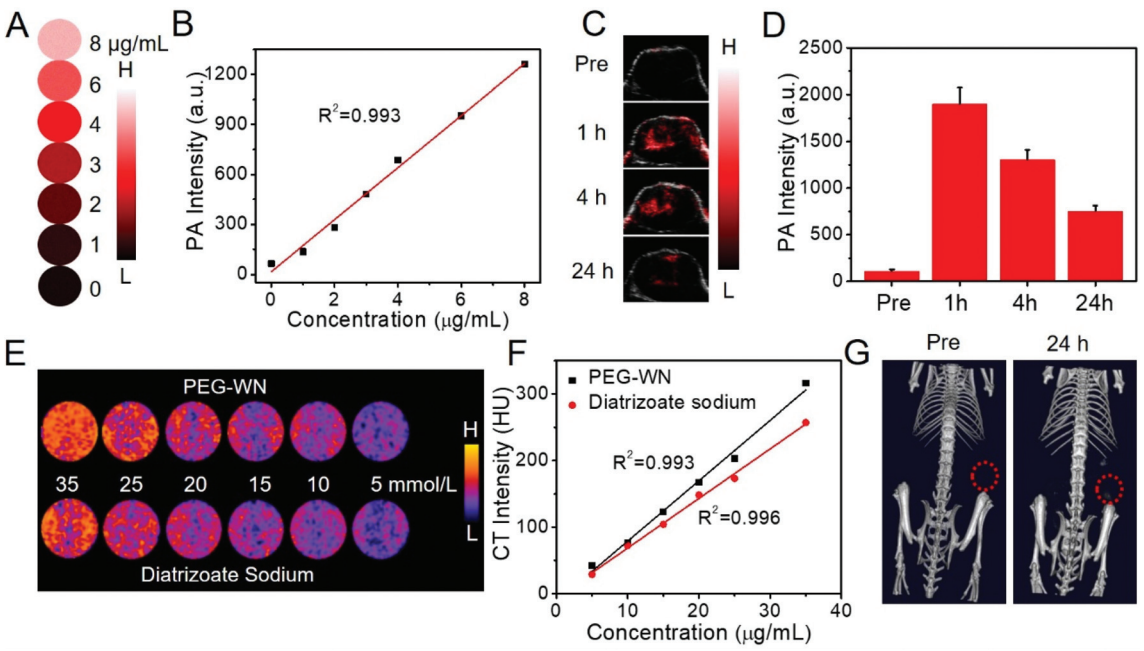

Fig. 4 (A) *In vitro* PA images and (B) signal intensities of PEG-WN NPs solution with different concentrations. (C) *In vivo* PA images of the tumor site before and after i.v. injection of PEG-WN NPs solution at different time points. (D) The intensities of PA signals corresponding to (C). (E) *In vitro* CT images and (F) signal intensities of PEG-WN NPs and diatrizoate sodium at different concentrations. (G) 3D *in vivo* CT images of CT26 tumor-bearing mouse before and after i.v. injection of PEG-WN NPs.

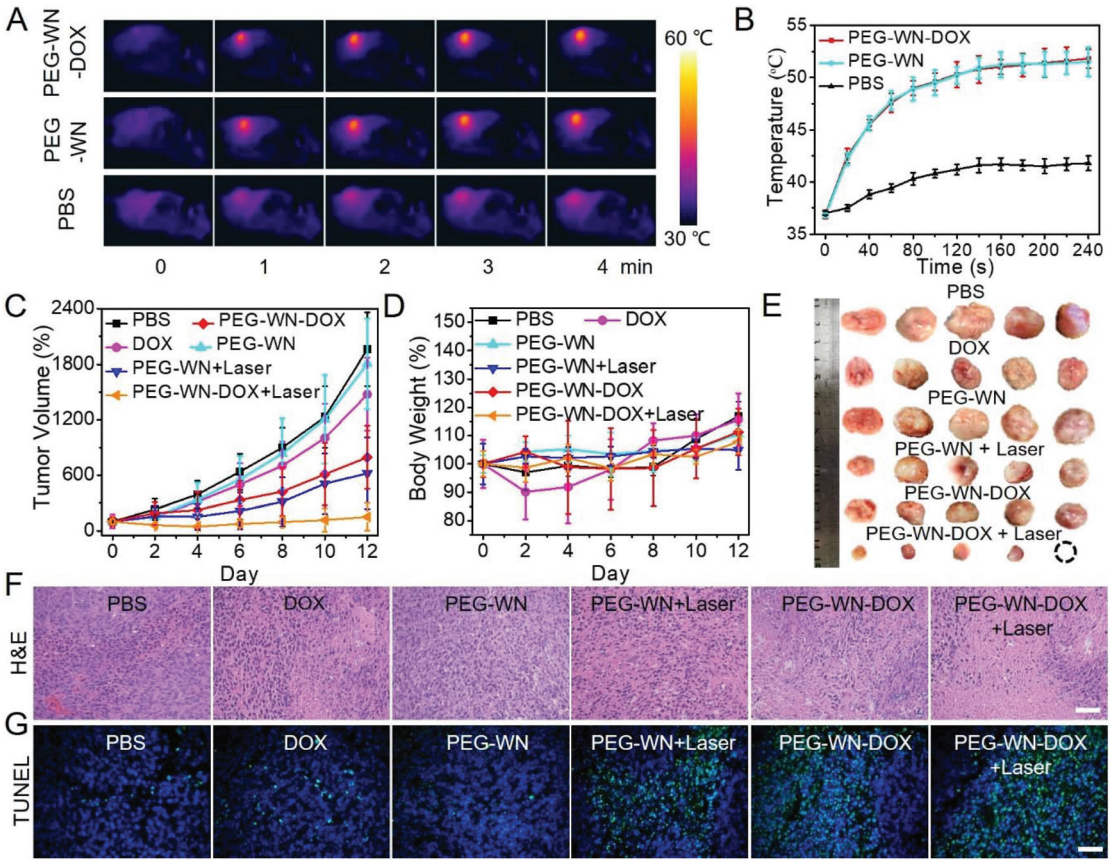

Fig. 5 (A) *In vivo* photothermal images and (B) the corresponding tumor temperature changes of mice after i.v. injection of PBS, PEG-WN and PEG-WN-DOX NPs. (C) Relative tumor volume and (D) body weight of mice of different groups. (E) Photographs of the harvested tumors after different treatments. (F) Images of H&E and (G) TUNEL immunofluorescence stained tumor sections (scale bar: 100 μm).

Next, the *in vivo* therapeutic effect of different treatments was evaluated. The tumor size and body weight of each group were measured every other day for 12 days. As shown in Fig. 5C, free DOX treatment induced a limited inhibition effect on tumor growth, while the tumor growth in the PEG-WN NPs + laser or PEG-WN-DOX NPs group was significantly suppressed. Besides, compared with free DOX, PEG-WN-DOX NPs showed a prolonged systemic circulation, which indicated the good performance of PEG-WN NPs as drug carriers (Fig. S12†). More impressively, the PEG-WN-DOX NPs + laser group, which combined PTT and chemical therapy, induced a maximum tumor inhibition effect. It is also worth mentioning that only the free DOX-treated group had an obvious body weight loss during the first few days of the treatment due to the toxic effect on the organisms while the weights of the other groups were basically stable (Fig. 5D). This also indirectly demonstrated the good delivery capacity of PEG-WN NPs as drug carriers, which was also verified by the fluorescence distribution of DOX in various organs from different groups (Fig. S13†). Besides, the tumor cell damage and apoptosis levels were further evaluated by hematoxylin and eosin (H&E) and terminal deoxynucleotidyl transferase-mediated dUTP-biotin nick-end labeling (TUNEL) assay. The results in Fig. 5F and G showed great agreement with the tumor growth curves shown in Fig. 5C and indicated that the synergistic treatment is the most powerful mode for primary tumor suppression. As we all know, cancer is usually accompanied by metastasis in the course of development. Due to the deep and vascular insufficiency of new metastasis sites, light and drug are usually difficult to penetrate and accumulate. The current practice is to combine chemo-phototherapy with immunotherapy, and the effect is good.

Body clearance and *in vivo* toxicity

Moreover, the time-dependent excretion was also investigated to study the *in vivo* metabolism of PEG-WN NPs. High levels of W were detected in feces and urine post PEG-WN NPs injection, which indicated that the liver and spleen might play important roles in the body clearance of PEG-WN NPs. The long-term detection showed that the excreted concentration of W decreased steadily over time and over 80% W was cleared from the body in one week (Fig. 6A). Meanwhile, the degradability of PEG-WN NPs has also been assessed. As shown in Fig. 6B and C, the PEG-WN NPs aqueous solution exposed to air exhibited a gradual decrease of absorbance and changed from black to light blue over time. Furthermore, no obvious

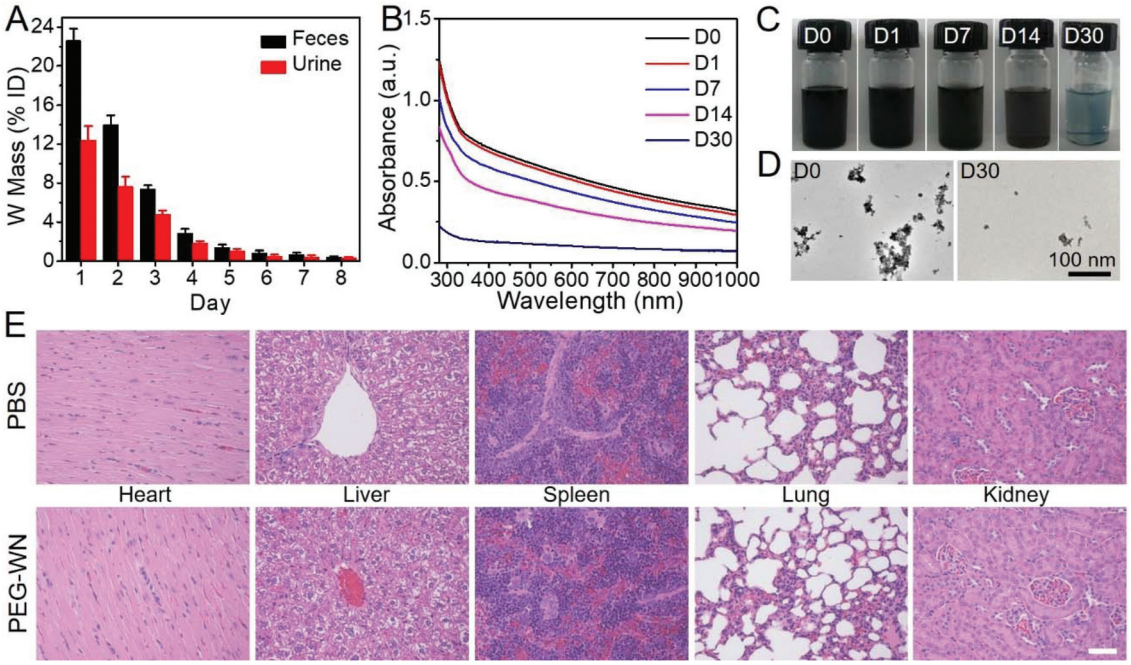

Fig. 6 (A) The W levels in feces and urine post i.v. injection of PEG-WN NPs. (B) UV/Vis-NIR absorbance spectra and (C) digital photos of PEG-WN solution (100 μg mL^{-1}) after exposure in air for various days. (D) TEM images of PEG-WN NPs at day 0 and after exposure in air for 30 days. (E) H&E-stained images of the major organs from treated mice (scale bar: 100 μm).

NPs were found in the TEM grid when PEG-WN NPs aqueous solution was exposed to air for 30 days (Fig. 6D). Obviously, the PEG-WN NPs underwent oxidative degradation. Then XPS analysis was used to analyze the oxidation mechanism. Most of the W element in the nanostructures was oxidized from the tungsten nitride to tungsten oxide state (Fig. S14†), indicating the formation of water-soluble small molecular species (for example, ammonium metatungstate hydrate). Thus, most of PEG-WN NPs *in vivo* could be excreted in one week, and the small remnant would be oxidized to water-soluble small molecular species. Both the body clearable and degradable behaviors highlight their great potential for applications in the clinic.

In addition, the mice were sacrificed after 12 days of treatment and the major organs were collected for H&E staining. No noticeable damage was observed in the major organs, such as the heart, liver, spleen, lung, and kidney (Fig. 6E and Fig. S15†). The blood biochemistry analysis results also indicated no potential side effect or toxicity to the normal tissues caused by PEG-WN NPs (Table S3†). These results make us believe that PEG-WN NPs could act as safe nano-agents for biomedical applications.

Conclusions

In summary, we constructed an effective and safe nanoplatform based on PEG-WN NPs for dual-modal imaging-guided combinatorial chemo-photothermal therapy. The PEG-WN NPs exhibited good water dispersibility, strong NIR absorbance and high photothermal conversion efficiency; thus they could be used as excellent PTAs for PTT. Such PTAs could also serve as drug carriers to realize a remarkable synergistic effect. Furthermore, the good PA/CT imaging capability of the PEG-WN NPs favors the precise positioning of the tumor for accurate treatment. In addition, no appreciable toxicity of PEG-WN NPs was observed *in vitro*/*vivo*, which confirmed their good biocompatibility. Considering the effective body clearance and biodegradable behaviors, the PEG-WN NPs hold great promise for clinical applications. Importantly, this work also for the first time demonstrates the unique advantages of WN nanostructures for *in vivo* tumor theranostic applications over other types of W-based nanostructures.

Experimental section

Materials

Tungstic acid (H_2WO_4) was purchased from Adamas Reagent Co., Ltd (Shanghai, China). Thiol poly(ethylene glycol) (SH-PEG) with a PEG molecular weight of 5000 was purchased from Ponsure Biotech, Inc. (Shanghai, China). (2-Hydroxypropyl)-β-cyclodextrin (β-CD) and 11-mercaptoundecanoic acid (MUA) were purchased from Innochem Technology Co., Ltd (Beijing, China). DOX·HCl was purchased from Meilun Biology Technology Co., Ltd (Dalian, China). Calcein-AM and propidium iodide (PI) were obtained from 4A Biotech Co., Ltd (Beijing, China). 3-[4,5-Dimethylthiazol-2-yl]-2,5-diphenyltetrazoliumbromide (MTT) was provided by Thermo Fisher (China). Roswell Park Memorial Institute (RPMI)

1640 medium and Dulbecco's modified Eagle's medium (DMEM) were purchased from Gibco Invitrogen Corp. All other reagents and solvents were used without further purification.

Preparation of WN NPs

H_2WO_4 was heated at 600 °C under an NH_3 flow (100 cm^3 min^{-1}). After cooling to room temperature, the prepared black WN sample was obtained and dispersed in deoxygenated DMSO solution, accompanied by sonication for 30 min in an ice-bath. The resulting supernatant was obtained by centrifugation at a speed of 6000 rpm for 10 min to remove large particles. The suspension was then washed with deionized water and stored at 4 °C for further modification.

Preparation of PEG-WN NPs

The PEG-WN NPs were prepared by reacting HS-PEG with WN NPs *via* the classic W–S bond. Briefly, 10 mg of HS-PEG was added into 20 mL of WN NPs solution (1 mg mL^{-1}) by sonication for 20 min and stirring overnight at room temperature. The unreacted HS-PEG was removed by centrifugation (11 000 rpm for 15 min). The as-prepared PEG-WN NPs were highly water-soluble and were stored at 4 °C before use.

Photothermal evaluation

To evaluate the photothermal effect of the as-prepared PWG-WN NPs, various concentrations of PWG-WN NPs samples were irradiated under an 808 nm laser; the temperature of the sample solution was recorded by using an FLIR camera at each predetermined time point. To evaluate the NIR stability of PEG-WN NPs, 40 μg mL^{-1} of PEG-WN NPs was irradiated at a power density of 1 W cm^{-2} for 8 min and then the laser was turned off. The procedure was repeated five times.

Drug loading and release

For loading of DOX, 11-mercaptoundecanoic acid-conjugated (2-hydroxypropyl)-β-cyclodextrin (MUA-CD) was synthesized *via* esterification in advance, which provides faithful loading sites.[38] Then MUA-CD was fixed on the surface of PEG-WN NPs through the W–S bond to prepare PEG-WN-CD NPs. After that 5 mg of demineralized DOX was added to the PEG-WN-CD NPs solution (20 mL, 1 mg mL^{-1}) and the mixture was stirred at room temperature for 24 h. The excess DOX was removed by centrifugation (11 000 rpm for 15 min). Finally, the obtained PEG-WN-DOX NPs solutions were stored at 4 °C for further use. The drug loading capacity was estimated to be 9.8% (w/w).

To investigate the pH-triggered drug release behavior of PEG-WN-DOX, 1 mL of PEG-WN-DOX NPs solution was encapsulated in a dialysis bag (MWCO = 14 000 Da) and immersed in 10 mL of acetate buffer solution (pH 5.0) or phosphate buffer solution (pH 7.4). Meanwhile, three parallel samples were prepared for each group, and all of them were incubated in a water bath at 100 rpm and 37 °C. The drug concentration in the release medium was detected by fluorescence at given time intervals.

Cell culture

The murine CT 26 and 4T1 cells were supplied by Procell Life Science & Technology Co., Ltd (Wuhan, China) and cultured in 1640 medium with 10% FBS and 1% antibiotics (penicillin–streptomycin, 10 000 U mL^{-1}) at 37 °C under a humidified atmosphere containing 5% CO_2.

In vitro cytotoxicity assay

In brief, CT 26 and 4T1 cells were seeded in 96-well plates at a density of 6000 cells per well, respectively. After incubation for 24 h, the cells were treated with PEG-WN NPs of various concentrations. For dark toxicity, the cells were further incubated for 24 h at 37 °C. For phototoxicity, after co-incubation with PEG-WN NPs for 4 h, the cells were irradiated with 808 nm laser (1 W cm^{-2}) for 5 min. After incubation for another 20 h, the cell viability was measured using the MTT assay.

Live/dead cell staining assay

CT26 cells were seeded in 6-well plates at a density of 5×10^5 cells per well and incubated at 37 °C for 24 h. Then the cells were incubated with PEG-WN NPs (50 μg mL^{-1}) for 4 h followed by 808 nm laser irradiation for 5 min. The cells treated with PEG-WN NPs or laser irradiation were tested as negative controls. Finally, all cells were stained with calcein-AM (4 μM) and PI (4 μM), incubated for 15 min at 37 °C, and then washed with PBS three times and visualized by using a fluorescence microscope (Olympus IX73, Japan).

Animals and tumor model

All animal studies were approved by the Institutional Animal Care and Use Committee (IACUC) of the Animal Experiment Center of Wuhan University (Wuhan, China). All mouse experimental procedures were performed in accordance with the Regulations for the Administration of Affairs Concerning Experimental Animals approved by the State Council of People's Republic of China. 5-Week-old female BALB/c mice were purchased from Wuhan University Animal Biosafety Lab and conventionally raised for a week. Each mouse was subcutaneously injected with 100 μL of CT26 tumor cells (~10^7 cells) in the right flank.

In vivo PA and CT imaging

For PA and CT imaging, the linearity between signal intensity and WN concentration *in vitro* was firstly evaluated. In brief, various concentrations of PEG-WN NPs were dispersed into PBS and then detected by multi-mode photoacoustic/ultrasonic imaging (Vevo LAZR) upon excitation at 808 nm to obtain the PA signal. Meanwhile, the same operation was performed on a Quantum FX microCT system (PerkinElmer) to collect the CT signal. For comparison, the CT signals of natrii diatrizoas at the same concentrations were collected as the control group. Next, for performing *in vivo* imaging, tumor-bearing mice were intravenously injected with PEG-WN NPs solution (6 mg kg^{-1}). After the injection, the signal intensity of PA and CT was obtained at predetermined time points through

multi-mode photoacoustic/ultrasonic imaging and using a Quantum FX microCT system, respectively. The signal before injection was used as the respective blank controls.

In vivo tumor temperature monitoring

8 h after intravenous injection of PBS, PEG-WN (6 mg kg^{-1}) and PEG-WN-DOX (6 mg kg^{-1} PEG-WN and 0.6 mg kg^{-1} DOX), tumor-bearing mice were irradiated with an 808 nm laser for 4 min (1.5 W cm^{-2}). The temperature of the tumor was monitored by using an FLIR Ax5 NIR thermal camera (FLIR Systems AB, Sweden).

Antitumor effect evaluation

When the tumor volume reached about 150 mm^3, mice were randomly divided into six groups. (1) PBS, (2) free DOX (0.6 mg kg^{-1}), (3) PEG-WN (6 mg kg^{-1}), (4) PEG-WN (6 mg kg^{-1}) + laser (1.5 W cm^{-2} for 4 min), (5) PEG-WN-DOX (6 mg kg^{-1} PEG-WN and 0.6 mg kg^{-1} DOX) and (6) PEG-WN-DOX (6 mg kg^{-1} PEG-WN and 0.6 mg kg^{-1} DOX) + laser (1.5 W cm^{-2} for 4 min). The laser irradiation was given 8 h after intravenous injection. The data of weight and tumor size were collected every other day. A digital Vernier caliper was used to measure the length and width of the tumor, and the tumor volumes were calculated according to the following formula: volume = length × $width^2/2$. When the treatment was finished, the relative body weight and tumor volume were determined as W/W_0 (where W_0 is the body weight before) and V/V_0 (where V_0 is the tumor volume before), respectively. Moreover, H&E-stained and TUNEL-stained tumor slices were obtained from the mice 24 h post various treatments.

Body clearance

Mice injected with PEG-WN NPs (6 mg kg^{-1}) were kept in metabolic cages to collect their feces and urine. The W level was detected by ICP-AES (Prodigy, USA).

In vivo system toxicity

Mice were sacrificed on the 12th day. The tumor and major organs were obtained and fixed with 4% formalin and embedded in paraffin after slicing for H&E staining. The blood samples were also taken on the 12th day for serum analysis.

Statistical analysis

The statistical analysis was conducted by Student's *t* test using Microsoft Excel 2010. The differences were considered to be statistically significant for P value < 0.05.

Conflicts of interest

The authors declare no competing financial interest.

Acknowledgements

This work was supported by the National Natural Science Foundation of China (51690152, 21721005).

References

1 Z. Meng, F. Wei, W. Ma, N. Yu, P. Wei, Z. Wang, Y. Tang, Z. Chen, H. Wang and M. Zhu, *Adv. Funct. Mater.*, 2016, **26**, 8231–8242.
2 H. Lin, X. Wang, L. D. Yu, Y. Chen and J. L. Shi, *Nano Lett.*, 2017, **17**, 384–391.
3 L. Li, C. Chen, H. Liu, C. Fu, L. Tan, S. Wang, S. Fu, X. Liu, X. Meng and H. Liu, *Adv. Funct. Mater.*, 2016, **26**, 4252–4261.
4 Y. Cai, P. Liang, Q. Tang, X. Yang, W. Si, W. Huang, Q. Zhang and X. Dong, *ACS Nano*, 2017, **11**, 1054–1063.
5 M. Qiu, D. Wang, W. Liang, L. Liu, Y. Zhang, X. Chen, D.-K. Sang, C. Xing, Z. Li, B. Dong, F. Xing, D. Fan, S. Bao, H. Zhang and Y. Cao, *Proc. Natl. Acad. Sci. U. S. A.*, 2018, **115**, 501–506.
6 S. H. Kim, I. In and S. Y. Park, *Biomacromolecules*, 2017, **18**, 1825–1835.
7 Y. Xing, J. Zhang, F. Chen, J. Liu and K. Cai, *Nanoscale*, 2017, **9**, 8781–8790.
8 L. Cheng, C. Wang, L. Feng, K. Yang and Z. Liu, *Chem. Rev.*, 2014, **114**, 10869–10939.
9 L. Dykman and N. Khlebtsov, *Chem. Soc. Rev.*, 2012, **41**, 2256–2282.
10 J. Shi, P. W. Kantoff, R. Wooster and O. C. Farokhzad, *Nat. Rev. Cancer*, 2017, **17**, 20–37.
11 R. Zhao, X. Han, Y. Li, H. Wang, T. Ji, Y. Zhao and G. Nie, *ACS Nano*, 2017, **11**, 8103–8113.
12 H. Zhu, Y. Wang, C. Chen, M. Ma, J. Zeng, S. Li, Y. Xia and M. Gao, *ACS Nano*, 2017, **11**, 8273–8281.
13 F. Lyu, Y. Zhang, R. N. Zare, J. Ge and Z. Liu, *Nano Lett.*, 2014, **14**, 5761–5765.
14 Y. Chen, L. Cheng, Z. Dong, Y. Chao, H. Lei, H. Zhao, J. Wang and Z. Liu, *Angew. Chem., Int. Ed.*, 2017, **56**, 1–7.
15 J. H. Park, L. Gu, G. V. Maltzahn, E. Ruoslahti, S. N. Bhatia and M. J. Sailor, *Nat. Mater.*, 2009, **8**, 331–336.
16 G. Maltzahn, J.-H. Park, A. Agrawal, N.-K. Bandaru, S.-K. Das, M.-J. Sailor and S.-N. Bhatia, *Cancer Res.*, 2009, **69**, 3892.
17 T. Yin, J. Liu, Z. Zhao, Y. Zhao, L. Dong, M. Yang, J. Zhou and M. Huo, *Adv. Funct. Mater.*, 2017, **27**, 1604620.
18 W. H. Chen, G. F. Luo, Q. Lei, S. Hong, W. X. Qiu, L. H. Liu, S. X. Cheng and X. Z. Zhang, *ACS Nano*, 2017, **11**, 1419–1431.
19 Q. Chen, L. Xu, C. Liang, C. Wang, R. Peng and Z. Liu, *Nat. Commun.*, 2016, **7**, 13193.
20 L. Cheng, J. Liu, X. Gu, H. Gong, X. Shi, T. Liu, C. Wang, X. Wang, G. Liu and H. Xing, *Adv. Mater.*, 2014, **26**, 1886–1893.

21 G. Tian, X. Zhang, X. Zheng, W. Yin, L. Ruan, X. Liu, L. Zhou, L. Yan, S. Li, Z. Gu and Y. Zhao, *Small*, 2014, **10**, 4160–4170.
22 Y. Yong, X. Cheng, T. Bao, M. Zu, L. Yan, W. Yin, C. Ge, D. Wang, Z. Gu and Y. Zhao, *ACS Nano*, 2015, **9**, 12451–12463.
23 Z. Chen, Q. Wang, H. Wang, L. Zhang, G. Song, L. Song, J. Hu, H. Wang, J. Liu, M. Zhu and D. Zhao, *Adv. Mater.*, 2013, **25**, 2095–2100.
24 G. Xi, S. Ouyang, P. Li, J. Ye, Q. Ma, N. Su, H. Bai and C. Wang, *Angew. Chem., Int. Ed.*, 2012, **51**, 2395–2449.
25 Z.-F. Huang, J. Song, L. Pan, F. Lv, Q. Wang, J.-J. Zou, X. Zhang and L. Wang, *Chem. Commun.*, 2014, **50**, 10959–10962.
26 P. Kalluru, R. Vankayala, C. S. Chiang and K. C. Hwang, *Angew. Chem., Int. Ed.*, 2013, **52**, 12332–12336.
27 Z. F. Huang, J. J. Song, L. Pan, X. W. Zhang, L. Wang and J. J. Zou, *Adv. Mater.*, 2015, **27**, 5309–5327.
28 J. Shi, Z. Pu, Q. Liu, A. M. Asiri, J. Hu and X. Sun, *Electrochim. Acta*, 2015, **154**, 345–351.
29 H. Yan, L. Wang, A. Wu, M. Meng, L. Zhao and H. Fu, *Angew. Chem., Int. Ed.*, 2015, **54**, 6325–6329.
30 Y. L. Wang, T. Nie, Y. H. Li, X. L. Wang, L. R. Zheng, A. P. Chen, X. Q. Gong and H. G. Yang, *Angew. Chem., Int. Ed.*, 2017, **56**, 7430–7434.
31 Y. Yong, X. Cheng, T. Bao, M. Zu, L. Yan, W. Yin, C. Ge, D. Wang, Z. Gu and Y. Zhao, *ACS Nano*, 2017, **9**, 12451–12463.
32 S. Zhu, L. Qian, M. Hong, L. Zhang, Y. Pei and Y. Jiang, *Adv. Mater.*, 2011, **23**, 84–89.
33 J. Hu, L. Xie, W. Zhao, M. Sun, X. Liu and W. Gao, *Chem. Commun.*, 2015, **51**, 11405–11408.
34 D. Li, Y. Ma, J. Du, W. Tao, X. Du, X. Yang and J. Wang, *ACS Nano*, 2017, **17**, 2871–2878.
35 M. E. Davis and M. E. Brewster, *Nat. Rev. Drug Discovery*, 2004, **3**, 1023–1035.
36 J. Weber, P. C. Beard and S. E. Bohndiek, *Nat. Methods*, 2016, **13**, 639–650.
37 Z. Zhou, B. Kong, C. Yu, X. Shi, M. Wang, W. Liu, Y. Sun, Y. Zhang, H. Yang and S. Yang, *Sci. Rep.*, 2014, **4**, 3653.
38 Y. Lu, Q. Hu, Y. Lin, D. B. Pacardo, C. Wang, W. Sun, F. S. Ligler, M. D. Dickey and Z. Gu, *Nat. Commun.*, 2015, **6**, 1006.